IEEE Access
Multidisciplinary | Rapid Review | Open Access Journal

Received October 29, 2019, accepted December 2, 2019, date of publication January 7, 2020, date of current version March 16, 2020.

Digital Object Identifier 10.1109/ACCESS.2020.2964603

Comparative Study of Discrete PI and PR Controls for Single-Phase UPS Inverter

MOHAMMAD PARVEZ[1], MOHAMAD FATHI MOHAMAD ELIAS[2], (Member, IEEE), NASRUDIN ABD RAHIM[2,3], (Senior Member, IEEE), FREDE BLAABJERG[4], (Fellow, IEEE), DEREK ABBOTT[1], (Fellow, IEEE), AND SAID F. AL-SARAWI[1], (Member, IEEE)

[1]School of Electrical & Electronic Engineering, The University of Adelaide, Adelaide, SA 5005, Australia
[2]Higher Institution Centre of Excellence, UM Power Energy Dedicated Advanced Centre, University of Malaya, Kuala Lumpur 59990, Malaysia
[3]Renewable Energy Research Group, King Abdulaziz University, Jeddah 21589, Saudi Arabia
[4]Institute of Energy Technology, Aalborg University, 9220 Aalborg, Denmark

Corresponding author: Mohammad Parvez (mohammad.parvez@adelaide.edu.au)

This work was supported in part by the School of Electrical and Electronic Engineering, University of Adelaide, SA, Australia, in part by the UM Power Energy Dedicated Advanced Centre (UMPEDAC), University of Malaya, under the Higher Institution Centre of Excellence (HICoE) Program, Ministry of Education, Malaysia, and in part by the Institute of Energy Technology, Aalborg University, Aalborg, Denmark

ABSTRACT This paper presents a comparative study of discrete proportional integral (PI) and proportional resonant (PR) current control for single-phase uninterruptible power supply (UPS) inverters. There is an increasing requirement for current and voltage-controlled UPS inverters with very low or zero steady-state error, improved transient response and lower total harmonic distortion (THD). The most promising type of current regulator for single-phase inverters is PR control because it can introduce an infinite gain at a selected resonance frequency such as the fundamental frequency to eliminate the steady-state error, which cannot be achieved by well-known proportional integral (PI) control. Note that PI control has limitations in terms of the steady-state magnitude and phase errors. In addition, PI control also has limited harmonic rejection capability, unlike the PR control, also can compensate for low-order harmonics. Imperfections in the current and voltage control scheme results in higher harmonic distortion of the output current and voltage. In this paper, performance of PR control parameters (K_p, K_i, and ω_c) and filter parameters (L_f and C_f) are optimally tuned to obtain a very low THD current with reduced output voltage ripple and steady-state error. The analysis, design and implementation of both PI and PR current control in single-phase UPS inverter applications through simulations and experiments are also presented in this paper. The performance of both of these control schemes are analyzed in terms of steady-state response, transient response, and level of current harmonics.

INDEX TERMS Proportional-integral (PI) control, proportional-resonant (PR) control, linear control, non-linear control, uninterruptible power supply (UPS), single-phase inverter, total harmonic distortion (THD).

I. INTRODUCTION

Present day uninterruptible power supplies (UPSs) are most popular due to clean power delivery to the varying load in all grid conditions. With today's advancement in power electronics, it is required to design UPS systems with high-quality outputs under extreme loading conditions for communications devices, medical equipment, and military equipment. Maintaining sinusoidal output requires voltage or current regulation to be incorporated into the UPS system, thus keeping the system output with low harmonic content for sustaining its performance, stability and reliability. According to the IEEE 1547 standard, minimum total harmonic distortion (THD) in the output voltage of UPS system must be maintained to less than 5% for nonlinear loads [1]–[3].

The current controlled UPS inverter is more commonly used compared to voltage control inverters. The control strategy involves two cascade or inner current loops, which are used to control the utility current, and an external voltage loop that is used to control the DC-link voltage. Current-based controllers can be divided into two major categories, namely, non-linear control technique and linear control technique.

The associate editor coordinating the review of this manuscript and approving it for publication was Snehal Gawande.

Several high performance of non-linear control schemes such as dead-beat control [4], [5], hysteresis control, predictive control [5], [6], iterative learning control [7], and sliding mode control have been implemented for UPS inverters [8], [9]. Among these control techniques, the dead-beat control technique belongs to the family of predictive regulators is the most commonly used control technique in several recent applications. When the deadbeat controller is optimally tuned, it provides faster transient response with close-to-zero tracking error in finite sampling steps. However, the dead-beat control is more prone to uncertainties, data mismatch and noise at high sampling frequency [10].

The hysteresis control method may be used in a voltage source inverter to compare the output utility current to the input reference current in order to generate switching signals for inverters. The benefits of hysteresis control are simplicity, self-dependent of load factors and good transient response [5], [11].

Predictive control method is well-known for its capability in nonlinear control systems. The predictive control technique can obtain precise current control with low total harmonic distortion (THD) and noise, but it is typically quite challenging for practical implementation [12], [13]. This control technique observes the inverter voltage needed to force the output utility current to follow a current reference.

On the other hand, the sliding mode (SM) control technique has gained more interest for both non-linear and linear loads [14]–[16]. The SM control technique is widely recognised as the algorithm of choice for implementing an inverter system because of its outstanding performance. The major benefits of this control is high dynamic response, stability, robustness, and easy implementation. On the other hand, the SM control technique has well known limitations when it is used with variable switching frequency, because it causes control imprecision, high power losses, and complex of output filter design. In order to overcome these limitations, rotating SM control [17], control strategy [18], and the SM control with fixed switching and variable width hysteresis compensator is proposed [19].

Currently, the SM control technique has been widely adapted due to its ability to AC tracing of the system's output [20]–[23]. Though, this control technique has decreased the harmonic level in the output, but it has limited rejection capability of high-order harmonics. The SM control with continuous-time control technique has been proposed in [24], [25], where the output filter current has been used as a state variable. Although, the SM control technique uses variable switching signal, it results in an undesirable chattering phenomenon. Hysteresis category switching has been considered for each leg of the inverter, resulting in further hardware complexity [26].

Linear control techniques, such as proportional integral (PI) control, repetitive control (RC) and proportional resonant (PR) control have been implemented in various power converters especially when tracking a sinusoidal signal for single-phase converters [5], [27]. Note that SM control

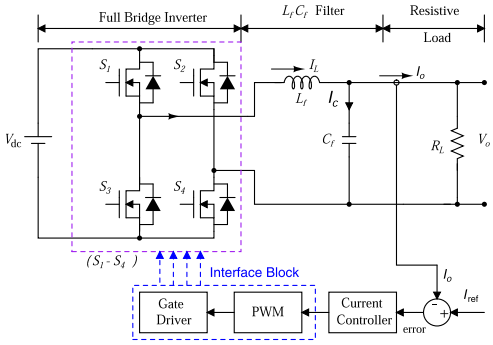

FIGURE 1. Single-phase inverter for UPS system with control strategy.

together with the proportional integral (PI) control technique has been proposed in [28], where the PI controller also well-known drawbacks such as being associated with a theoretically infinite gain, and it is unable to track a sinusoidal reference with steady state error. Therefore, the performance of this controller in an inverter is not adequate. The repetitive control (RC) was built based on internal model principle (IMP), which is able to minimize steady-state error by periodically settling its parameters resulting in excellent harmonic rejection capability [29], [30]. However, it is rather problematic, exhibiting a slow dynamic response that affects its stability.

Over the last decade, PR control has gained dominance in current regulation for stand-alone or grid-connected converters, which are able to track a sinusoidal current reference with minimal steady-state and phase error. Note that PR control can achieve a large gain around the resonance frequency spectrum, depending on the value of resonance gain K_r [31] whilst improving the system stability.

This paper considers both PI and PR current control techniques, focusing on single-phase UPS inverter systems. Among the control techniques, two of them have been selected for comparison in terms of performance that are proportional integral (PI) and proportional resonant (PR), taking into account their significance and also practical implementation. A single-phase inverter for the UPS system connected to the load through an $L_f C_f$ filter with a control strategy is shown in Figure 1, where $V_{\rm dc}$ is the inverter input DC voltage, V_o is the output voltage, L_f is the filter inductance, C_f is the filter capacitance, and R_L is the load resistor. Note that I_L is the filter current through the inductor, I_C is the filter current through the capacitor, and I_o is the output current through the resistor.

II. CURRENT CONTROL USING PI AND PR CONTROLLERS

For comparison, both the closed-loop transfer functions of the PI and PR current controllers are analyzed. The block diagram of closed-loop PI and PR current control scheme used for the comparison are shown in Figures 2 and 3.

The closed-loop transfer function of the system using PI controller can be defined by

$$M_{\rm PI}(s) = \frac{I_o}{I_{\rm ref}} = \frac{G_{\rm PI}(s)G_I(s)G_F(s)}{1 + G_{\rm PI}(s)G_I(s)G_F(s)}, \qquad (1)$$

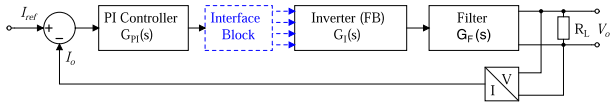

FIGURE 2. Block diagram of closed-loop PI control scheme.

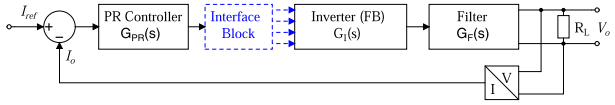

FIGURE 3. Block diagram of closed-loop PR control scheme.

where $G_{\mathrm{PI}}(s) = K_p + \frac{K_i}{s}$, $G_I(s) = K$ and $G_F(s) = \frac{R_L}{R_L L_f C_f s^2 + L_f s + R_L}$ are the transfer functions of the PI controller, the inverter, and the filter including the load, respectively. Substituting all the transfer functions yields the complete transfer function of the system that is represented by

$$M_{\mathrm{PI}}(s) = \frac{K(K_p s + K_i)}{L_f C_f s^3 + \frac{L_f}{R_L} s^2 + (1 + KK_p)s + KK_i}. \quad (2)$$

Similarly, the closed-loop transfer function of the system using PR controller can be defined by

$$M_{\mathrm{PR}}(s) = \frac{I_o}{I_{\mathrm{ref}}} = \frac{G_{\mathrm{PR}}(s)G_I(s)G_F(s)}{1 + G_{\mathrm{PR}}(s)G_I(s)G_F(s)}, \quad (3)$$

where $G_{\mathrm{PR}}(s) = K_p + K_i \frac{2\omega_c s}{s^2 + 2\omega_c s + \omega_o^2}$, $G_I(s) = K$, and $G_F(s) = \frac{R_L}{R_L L_f C_f s^2 + L_f s + R_L}$ are the transfer functions of the PR controller, the inverter, and the filter including the load, respectively. The complete transfer function of the system can be obtained by

$$M_{\mathrm{PR}}(s) = \frac{K\{K_p s^2 + 2(K_p\omega_c + K_i\omega_c)s + K_p\omega_o^2\}}{\lambda_4 s^4 + \lambda_3 s^3 + \lambda_2 s^2 + \lambda_1 s + \lambda_o}, \quad (4)$$

where

$$\lambda_4 = L_f C_f;$$
$$\lambda_3 = (\frac{L_f}{R_L} + 2\omega_c L_f C_f);$$
$$\lambda_2 = (1 + 2\omega_c \frac{L_f}{R_L} + L_f C_f \omega_o^2 + KK_p);$$
$$\lambda_1 = (2\omega_c + \omega_o^2 \frac{L_f}{R_L} + 2KK_p\omega_c + 2KK_i\omega_c); \text{ and}$$
$$\lambda_o = \omega_o^2 + KK_p\omega_o^2.$$

Figure 4 shows the frequency responses of the closed-loop PI and PR current control systems. As can be seen from the figure, the PR controller maintains its stability where the phase is always kept below 180 deg. The bandwidth can be widened by tuning ω_c appropriately, which can helpful to reduce sensitivity towards slight frequency variation [27].

III. CONTROLLER TUNING USING BODE DIAGRAMS AND PHASE MARGIN CRITERION

The tuning of controller parameters is normally performed by using Bode diagrams and the phase margin criterion,

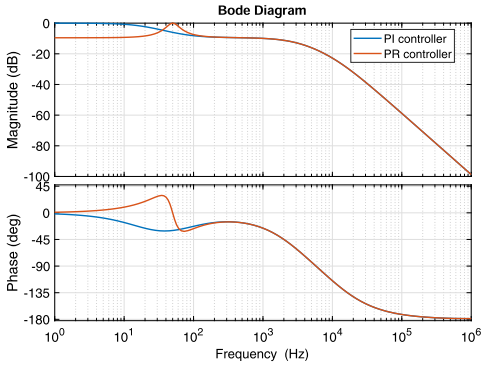

FIGURE 4. Frequency response of closed-loop transfer function using PI controller ($K_p = 0.5$, and $K_i = 200$); and using PR controller ($K_p = 0.5$, $K_i = 1000$, $\omega_o = 314$ rad/s, and $\omega_c = 0.1$ rad/s).

and via analyzing the stability by means of the phase margin at the crossover frequency defined by the proportional gain. In many applications, analysis using Bode diagrams is enough to achieve required results. A more systematic method by means of Nyquist diagrams can also be used to tune the controller parameters, which can give higher stability and improved performance.

In order to investigate the effect of controller parameters on the non-ideal PR controller performance, one of the parameters will be varied while the other parameters will be kept constant. When $K_i = 1$, $\omega_c = 1$ rad/s, and the proportional gain K_p is varied, the magnitude of PR controller increases, but the phase of PR controller decreases, as shown in Figure 5 (a). Figure 5 (b) shows the frequency response of the controller in terms of the magnitude and phase when K_i is varied while $K_p = 0$, and $\omega_c = 1$ rad/s. It can be observed that the magnitude of the PR controller gain increases when K_i is increased. But K_i has no effect on the bandwidth of the system as seen from the phase response of the PR controller.

Assuming $K_p = 0$ and $K_i = 1$, a change in ω_c has an effect on both the magnitude and the phase of the PR controller. Both the magnitude and the phase increase when ω_c is increased, as shown in Figure 5 (c).

The frequency response of this controller with several gain constants K_p and K_i (normally, $0 < K_p < 1$, and $100 < K_i < 2000$ as mentioned in [32]) are shown in Figure 5 (a) and (b), respectively. The controller parameters K_p and K_i are determined to achieve a reasonable closed-loop response, steady-state and transient performance. The reasonable K_p gives to the superior tracking performance. A higher value of K_i leads to faster response with better current harmonics rejection but a higher bandwidth and phase margin. Therefore the reasonable value of K_i can be chosen according to the desired bandwidth and phase margin. A higher value of ω_c increases the peak magnitude at the fundamental frequency, corresponding to higher gain and better ripple attenuation. A small value of ω_c gives rise to a wider bandwidth at the fundamental frequency.

The basic PR controller design requirements are as follows [27], [32].

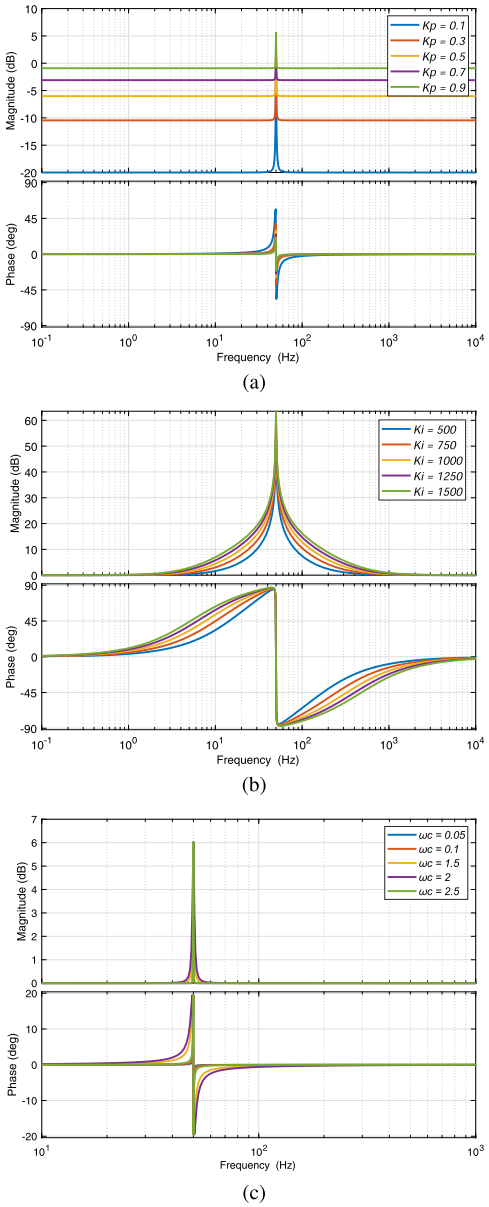

FIGURE 5. Frequency response of non-ideal PR controller as a function of (a) K_P changes, (b) K_i changes, and (c) ω_c changes.

- A suitable ω_c should be selected to provide a reasonable bandwidth around the resonance frequency.
- The proportional gain constant K_p is then should be selected to ensure that superior performance in sinusoidal reference tracking could be attained.
- Finally, K_i should be selected so that the steady-state errors in both magnitude and phase are eliminated.

IV. CONTROLLERS TUNING USING AUTO OPTIMIZATION

To verify the model and controllers performance, auto optimization technique can also be analyzed in MATLAB system. Converters are non-linear systems which analysis, control, and auto optimization could be difficult. Linear techniques based on classical controller have problems related to the stability around the operation point. Non-linear controllers such as: PI and PR controllers can be implemented to improve the stability of the converter, but such techniques could be complex. Since model can be linearized before auto optimization. The algorithm of controllers tuning using auto optimization technique as shown in Figure 6.

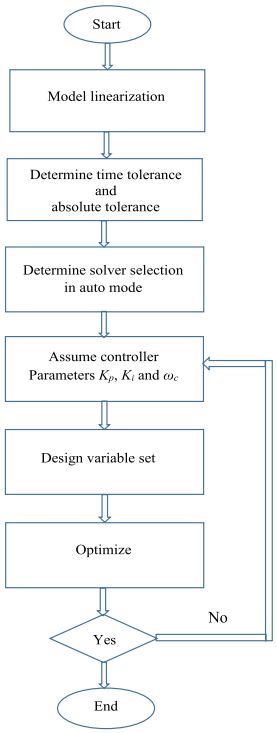

FIGURE 6. Algorithm of controllers tuning using auto optimization.

V. CONTROLLER PERFORMANCE ANALYSIS FOR OPEN-LOOP SYSTEM

According to simulations shown in Figure 5, the design requirement for the current controllers resonable bandwidth, harmonic rejection capability, higher tracking response, and frequency variation range from 48 to 51 Hz, the controller parameters are selected as; $K_p = 0.5$, $K_i = 1000$, and $\omega_c = 0.1$ rad/s. Figure 7 shows the frequency response of non-ideal PR controller in MATLAB using the selected values where Figure 8 represents the frequency response using auto optimization values. It should be noted from Figure 7 that the transfer function of open loop non-ideal PR controller shows that the gain margin of the system is finite, and the phase margin of the system is 79.3° (leading), and 76.4° (lagging) at under frequency (48 Hz), and over frequency (51 Hz), respectively.

VI. CONTROLLER PERFORMANCE ANALYSIS FOR CLOSED-LOOP SYSTEM

Typically, a closed-loop system attains improved stability compared to an open loop system, since it has better disturbance rejection capability. Although the PR controller has more advantages over PI controllers, its closed-loop performance can be affected by a various factors such as grid

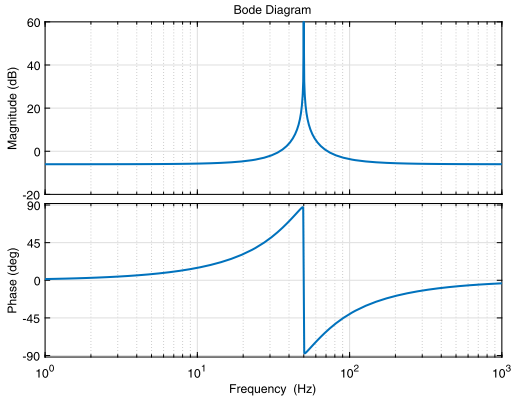

FIGURE 7. Frequency response of non-ideal PR controller using the selected values ($K_p = 0.5$, $K_i = 1000$, and $\omega_c = 0.1$ rad/s).

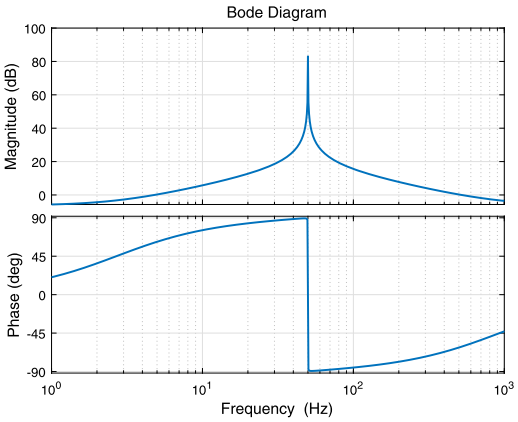

FIGURE 8. Frequency response of non-ideal PR controller using auto optimization values ($K_p = 0.4856$, $K_i = 14164$, and $\omega_c = 0.1$ rad/s).

frequency variation. When the fundamental frequency of the PR controller varies, the expected output will be attenuated and will contain a phase error. The effect of frequency variation is not analyzed on the PI controller since its output system is unstable.

In addition, the effect of frequency variation can be seen in Figure 4, where the PR controller maintains its stability where the phase margin of the system is 15.1° (leading), and 3.46° (lagging) at under frequency (48 Hz), and over frequency (51 Hz), respectively. For a more realistic analysis, the frequency responses of closed-loop PI and PR controllers using auto optimization values are shown in Figure 9 where the target frequency variation is attained and phase error highly attenuated.

A. IMPLEMENTATION OF PI CONTROLLER USING DISCRETE TRANSFER FUNCTION

The discrete transfer function of the PI controller can be obtained by applying the bilinear transformation and substituting $s = \frac{2(z-1)}{T(z+1)}$ into in $G_{\mathrm{PI}}(s) = K_p + \frac{K_i}{s}$. This yields the following transfer function in z-domain;

$$G_{\mathrm{PI}}(z) = \frac{(K_p + K_i\frac{T}{2}) + (-K_p + K_i\frac{T}{2})z^{-1}}{1 - z^{-1}} \tag{5}$$

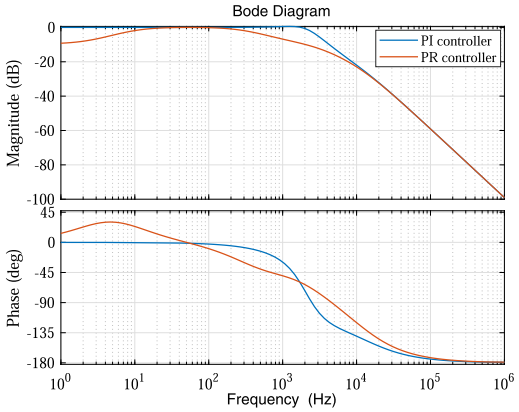

FIGURE 9. Frequency response of closed-loop transfer function using PI controller ($K_p = 0.4856$, and $K_i = 14164$); and using PR controller ($K_p = 0.4856$, $K_i = 14164$, $\omega_o = 314$ rad/s, and $\omega_c = 0.1$ rad/s).

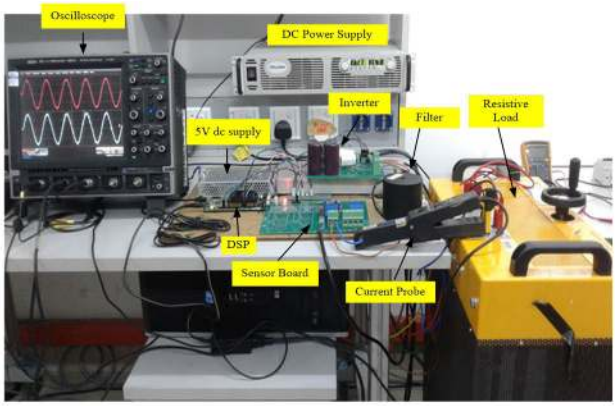

FIGURE 10. Experimental set up.

$$G_{\mathrm{PI}}(z) = \frac{b_0 + b_1 z^{-1}}{a_0 + a_1 z^{-1}}, \tag{6}$$

where T is the sampling time and: $b_o = K_p + K_i\frac{T}{2}$, $b_1 = -K_p + K_i\frac{T}{2}$, and $a_0 = 1$.

Finally, the difference equation of PI controller becomes

$$u(n) = b_0 e(n) + b_1 e(n-1) - a_1 u(n-1), \tag{7}$$

where $u(n)$ is the present controller output, $u(n-1)$ is the previous controller output, $e(n)$ is the present error, and $e(n-1)$ is the previous error.

Based on the optimized PI controller parameters ($K_p = 0.5$ and $K_i = 200$), the coefficients of the PI controller become, $b_0 = 0.505$, $b_1 = -0.995$, and $a_1 = -1$. The transfer function in z-domain PI controller is given by

$$G_{\mathrm{PI}}(z) = \frac{0.505 - 0.995z^{-1}}{1 - z^{-1}}. \tag{8}$$

B. IMPLEMENTATION OF PR CONTROLLER USING DISCRETE TRANSFER FUNCTION

The discrete transfer function of the non-ideal PR controller can be obtained by applying bi-linear transformation and

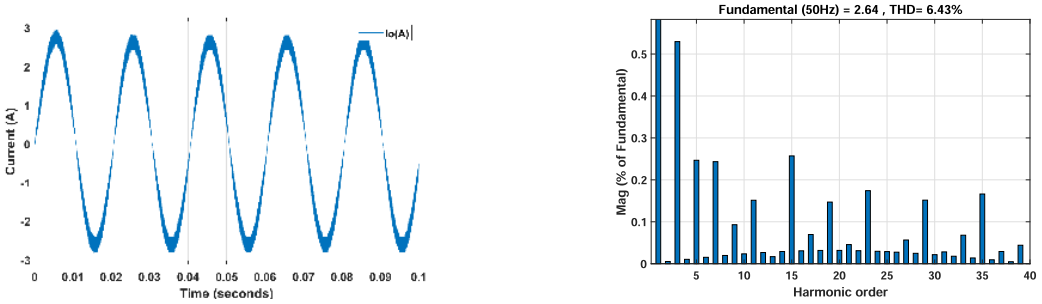

(a) Load current (b) FFT analysis of THD

FIGURE 11. Simulation results of load current and FFT analysis of THD using selected values from Bode plot and phase margin criterion for PI controller ($K_p = 0.5$, and $K_i = 200$).

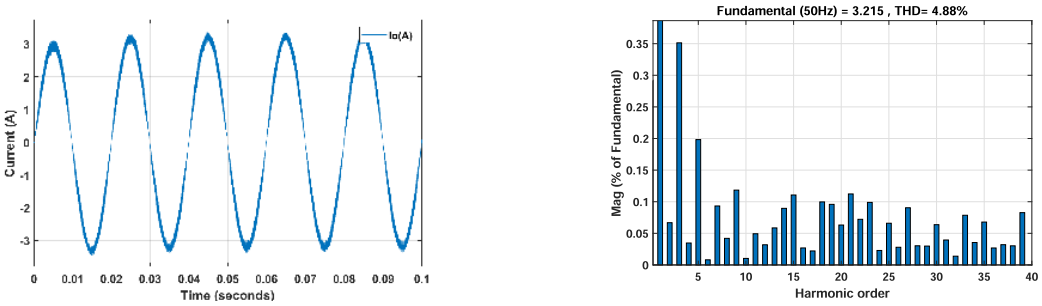

(a) Load current (b) FFT analysis of THD

FIGURE 12. Simulation results of load current and FFT analysis of THD using selected values from Bode plot and phase margin criterion for PR controller ($K_p = 0.5$, and $K_i = 1000$).

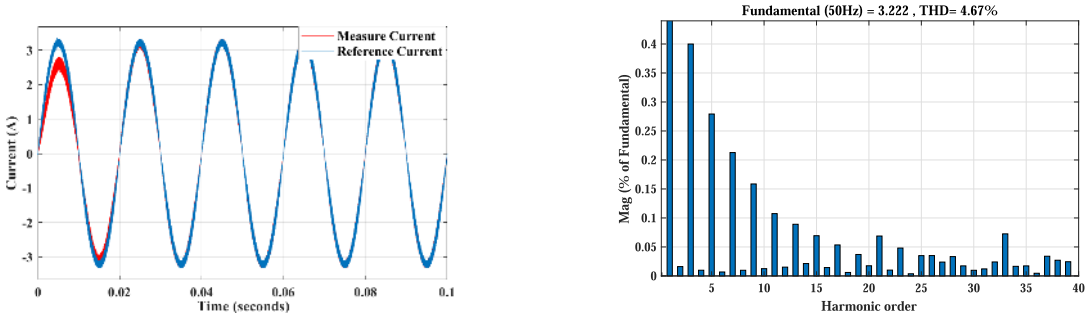

(a) Load current (b) FFT analysis of THD

FIGURE 13. Simulation results of load current and FFT analysis of THD using auto optimization values for PI controller ($K_p = 0.4856$, and $K_i = 14164$).

putting $s = \frac{2(z-1)}{T(z+1)}$ into in $G_{\mathrm{PR}}(s) = K_p + K_i \frac{2\omega_c s}{s^2+2\omega_c s+\omega_o^2}$. This yields the following transfer function in the z-domain;

$$G_{\mathrm{PR}}(z) = K_p + \frac{2K_i\omega_c \frac{2(z-1)}{T(z+1)}}{\frac{4(z-1)^2}{T^2(z+1)^2} + 2\omega_c \frac{2(z-1)}{T(z+1)} + \omega_o^2}, \tag{9}$$

where T is the sampling time. Equation (9) can be rearranged in the following form in terms of the controller's output $U(z)$ and the error $E(z)$,

$$G_{\mathrm{PR}}(z) = \frac{U(z)}{E(z)} = \frac{b_0 + b_1 z^1 + b_2 z^{-2}}{a_0 + a_1 z^{-1} + a_2 z^{-2}}, \tag{10}$$

where

$$b_0 = \frac{(4 + 4T\omega_c + \omega_o^2 T^2)K_p + 4K_i T\omega_c}{4 + 4T\omega_c + \omega_o^2 T^2},$$

$$b_1 = \frac{(2\omega_o^2 T^2 - 8)K_p}{4 + 4T\omega_c + \omega_o^2 T^2},$$

$$b_2 = \frac{(4 - 4T\omega_c + \omega_o^2 T^2)K_p - 4K_i T\omega_c}{4 + 4T\omega_c + \omega_o^2 T^2}, \quad a_0 = 1,$$

$$a_1 = \frac{2\omega_o^2 T^2 - 8}{4 + 4T\omega_c + \omega_o^2 T^2}, \quad \text{and}$$

$$a_2 = \frac{4 - 4T\omega_c + \omega_o^2 T^2}{4 + 4T\omega_c + \omega_o^2 T^2}.$$

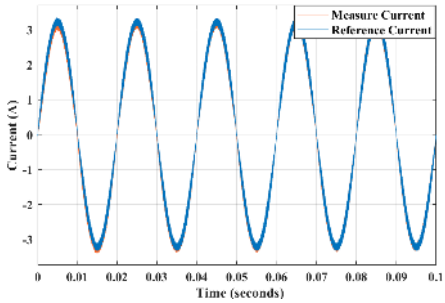

(a) Load current

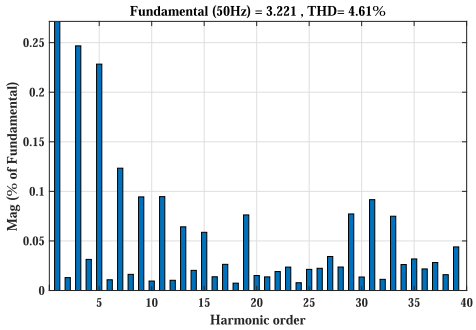

(b) FFT analysis of THD

FIGURE 14. Simulation results of load current and FFT analysis of THD using auto optimization values for PR controller ($K_P = 0.4856$, and $K_i = 14164$).

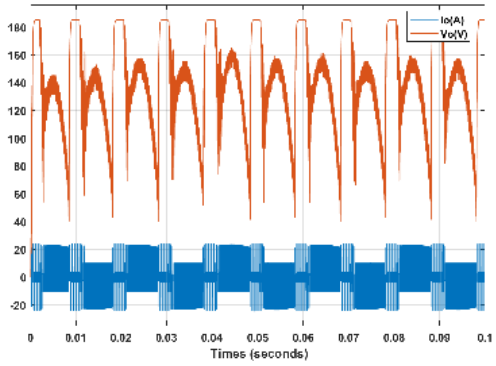

FIGURE 15. Simulation results of output voltage and current using non-linear load for PR controller.

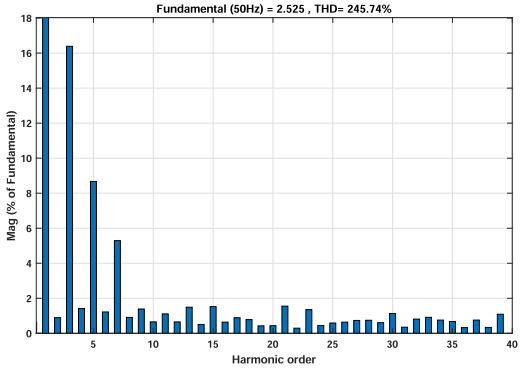

FIGURE 17. Simulation result of FFT analysis of current THD using non-linear load for PR controller.

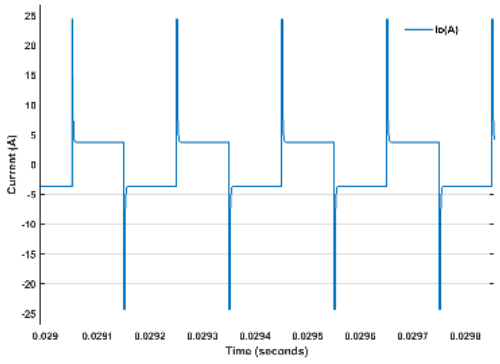

FIGURE 16. Simulation result of output current with zoom using non-linear load for PR controller.

Finally, the difference equation of the PR controller for hardware implementation is given by

$$u(n) = b_0 e(n) + b_1 e(n-1) + b_2 e(n-2) - a_1 u(n-1) - a_2 u(n-2). \quad (11)$$

Based on the optimized PR controller parameters ($K_p = 0.5$, $K_i = 1000$ and $\omega_c = 0.1$ rad/s), the coefficients of the PR controller become, $b_0 = 0.504999$, $b_1 = -0.99987$, $b_2 = 0.494995$, $a_0 = 1$, $a_1 = -1.9997$, and $a_2 = 1$.

The transfer function in the z-domain of the PR controller is given by

$$G_{\mathrm{PR}}(z) = \frac{U(z)}{E(z)} = \frac{0.504999 - 0.99987z^{-1} + 0.494995z^{-2}}{1 - 1.9997z^{-1} + z^{-2}}. \quad (12)$$

VII. DESIGN AND SETUP

The experimental prototype for testing the performance of both PI and PR current controllers is shown in Figure 10, with the inverter parameters are given in Table 1. The inverter is connected to the resistive load through the LC filter. For implementation of both controllers' algorithms, a 32-bit floating-point TMS320F28335 eZdsp development board is used. The C program for both controllers was developed using Texas Instrument Code Composer Studio 6.0 (CCS) software. The inverter switching frequency is set to 20 kHz and the dead-band time is set $t_{\mathrm{d1}} = 1.3\mu$s for the switching frequency, since the load is less inductive. The PWM pulses are generated through the internal PWM module of the DSP. Voltage and current signals are measured by using the 12-bit analog-to-digital converter (ADC) built inside the eZdsp development board. A sinusoidal reference signal is generated by sensing the grid voltage and using the

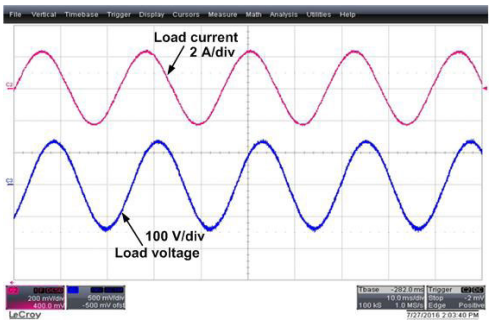

(a) Load current and voltage

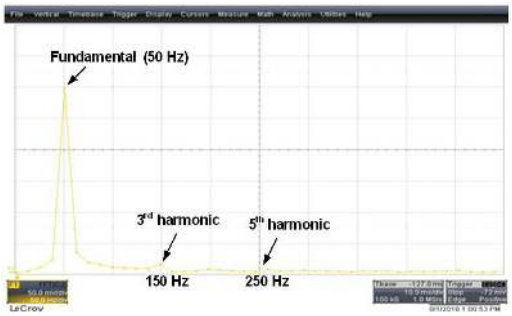

(b) FFT analysis of load current

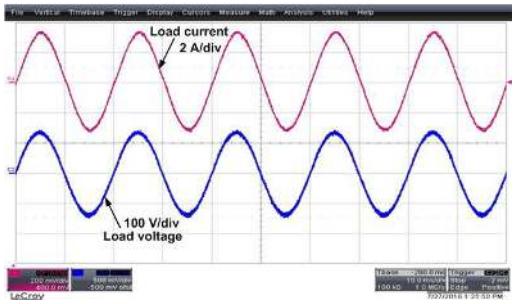

(c) Load current and voltage

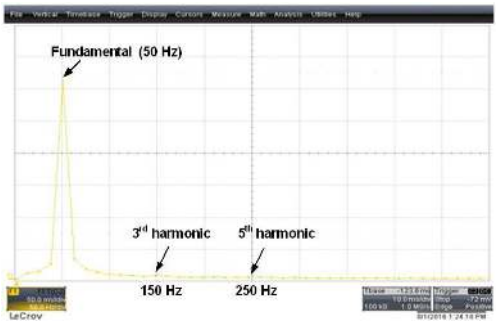

(d) FFT analysis of load current

FIGURE 18. Experimental results: (a) Load current, load voltage, and (b) FFT analysis of load current using PI controller; and (c) Load current, load voltage, and (d) FFT analysis of load current using PR controller.

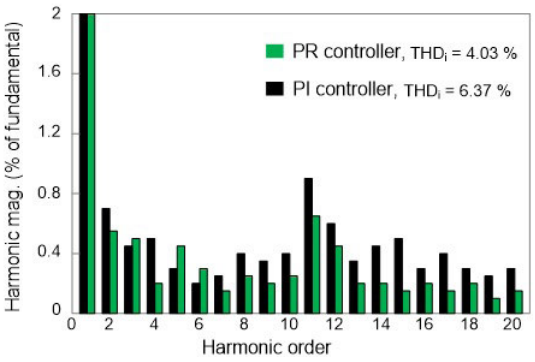

FIGURE 19. Total harmonic distortion (THD) of load current using PI and PR controller.

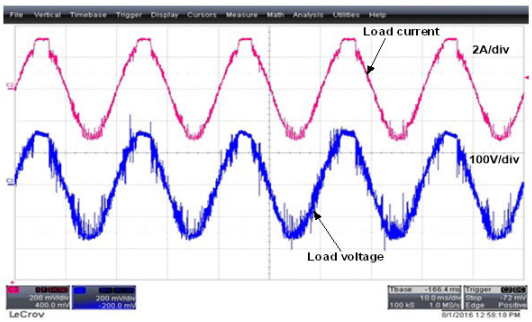

FIGURE 20. Experimental results of load current and load voltage using PI controller ($K_P = 0.7$ and $K_i = 200$).

TABLE 1. Inverter specifications.

Parameters	Value
DC voltage, V_{dc}	180 V
IGBT Module (S1-S4)	INFINEON (F4-50R06W1E30)
Voltage transducer	LEM LV25 – P
Current transducer	LEM LA25 – NP
Filter inductor, L_f	5 mH
Filter capacitance, C_f	0.22 μF
Resistor, R_L	50 Ω
Proportional gain constant, K_p	0.5
Integral gain constant, K_i	200 and 1000 for PI and PR, respectively
Cut-off frequency, ω_c	0.1 rad/s
Switching frequency, f_s	20 kHz

phase-locked-loop module. The power electronic switches used were IGBT-based modules.

VIII. RESULTS AND DISCUSSION

The simulation and experiment implementation results of discrete PI and PR current controllers for a single-phase UPS inverter are presented. MATLAB/SIMULINK®software is used for the simulation. The performance of both controllers is compared in terms of the steady-state response, transient response, and current total harmonic distortion (THDi). The control parameters are selected from the simulation are used for experimental verification. The experimental is demonstrated through a 250 W inverter operating at an RMS voltage of 110 V. The RMS current is therefore equal to 2.27 A with 3.21 A peak value.

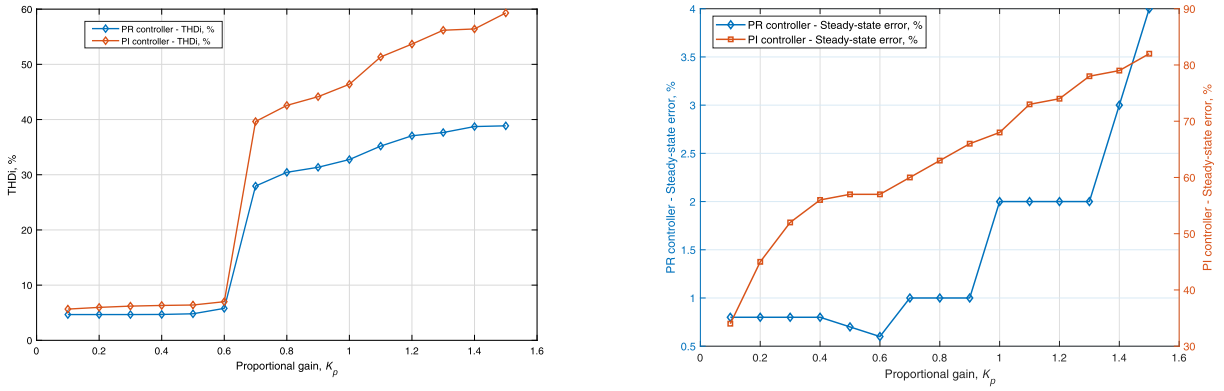

(a) (b)

FIGURE 21. THDi and Steady-state error changes with the change in K_p for both PI and PR controller (a) THDi versus K_p, and (b) Steady-state error versus K_p.

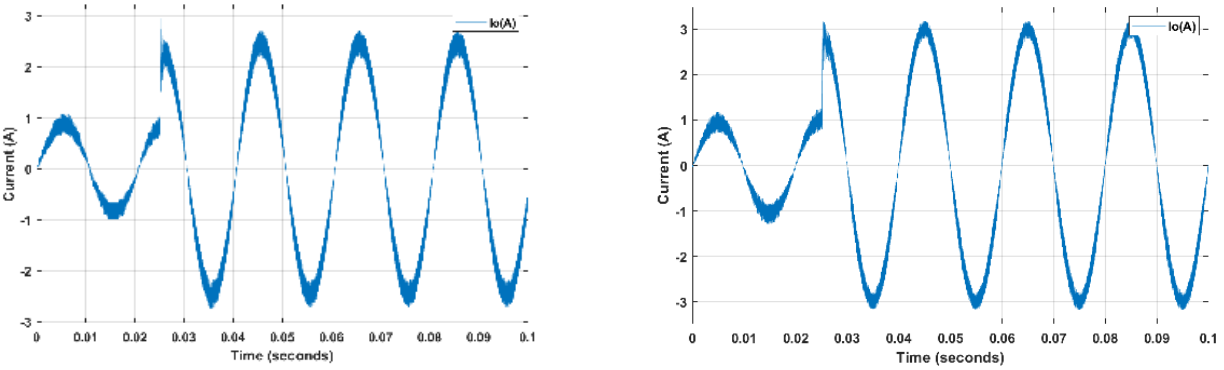

(a) (b)

FIGURE 22. Simulation results showing the transient response in load current (a) using by the PI controller, and (b) using by the PR controller.

A. STEADY-STATE RESPONSE OF PI AND PR CONTROLLER

The controller parameters of K_p, K_i, and ω_c have been optimally set for UPS inverter. The simulation results of load current and FFT analysis of THD value are shown in Figures 11 and 12. When using the PI controller, FFT analysis on the load current yields a THD value of 6.43% as shown in Figure 11 (b), whereas FFT analysis on the load current yields a THD value of 4.88% using by the PR controller. These results indicate that the current harmonics have been well suppressed by the PR controller as shown in Figure 12 (b).

The simulation results of load current and FFT analysis of THD using auto optimization values are shown in Figures 13, and 14. It can be observed from Figure 13 when using auto optimization values in the PI controller, although a lower THD value is acheived, the current response is relatively slow. After a certain time the current reaches steady-state. On the other hand, Figure 14 shows a faster current response, improved tracking performance and low THD when using auto optimization values in the PR controller.

In addition, to observe the performance of the PR controller in a non-linear load, steady-state non-linear load tests are performed using an uncontrolled full bridge diode rectifier within a MATLAB simulation. The rectifier is used between the inverter output and load. The simulation results of output voltage, current, and FFT analysis of current THD using the non-linear load with the PR controller are presented in Figures 15, 16, and 17. With a non-linear load the increase in output current THD is within the tolerable limits specified in the IEC 62040-3 standard.

The experimental results showing load current, load voltage, and FFT analysis of load current are given in Figure 18. From 18 (a), the load current only reaches 2.8 A peak, which represents an error of 12.77% from the reference current $I_{\text{ref}} = 3.21$ A peak. Both experiment and simulation results of load current show that steady-state error occurs when using the PI controller. From 18 (c), the load current reaches a maximum of 3.21 A peak of the current reference when using the PR controller. It is clear that the load current achieves zero steady-state error as compared to PI controller, of 12.77%. The FFT analysis of the load current for both the PI and PR controller are shown in Figure 18 (b) and (d), respectively. It can be seen from Figure 18 (d), when using the PR controller the magnitudes of 3$^{\text{rd}}$ and 5$^{\text{th}}$ harmonics were found

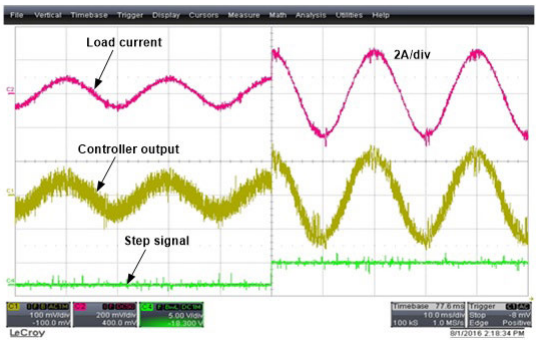

FIGURE 23. Experimental results showing the transient response in load current, controller output, and step signal using by the PI controller ($K_p = 0.5$, and $K_i = 200$).

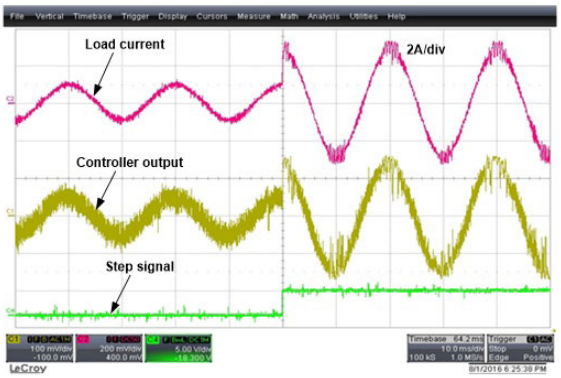

FIGURE 24. Experimental results showing the transient response in load current, controller output, and step signal using by the PI controller ($K_p = 0.7$, and $K_i = 300$).

to be very low as compared to those of the PI controller in Figure 18 (b).

Moreover, the harmonic rejection capability of the PI controller and the PR controller is compared, as shown in Figure 19. It can be observed that the PR controller can obtain an overall current THD level lower than 5%, and individual harmonics level lower than 4%, that are meet in IEEE standards requirments [33].

When the value of K_p is increased ($K_p = 0.7$) for PI controller, the results of load current and voltage are shown in Figure 20. The current reaches the maximum of 3.21 A peak, but it is over modulated with more ripple in the output current and voltage, and therefore an increased 3rd harmonic level is observed.

Note that the optimal selection of K_p is most significant for both THD and the steady-state condition. The dependence of the THD on K_p and how that impacts the stead-state error is shown in Figure 21. It can be observed from Figure 21 (a), when the value of K_p is increased from 0.1 to 0.6, the THD slightly increases for both PI and PR controllers. On the other hand, when K_p is increased from 0.6 to 1.5, the output is more distorted resulting in greater THD. Figure 21 (b) shows the higher steady-state error for the PI controller when the value of K_p is increased from 0.1 to 1.5. The error value is below 1% for K_p between 0.1 and 0.6, with an increased value of

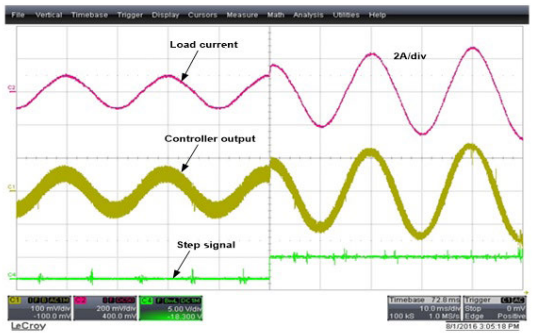

FIGURE 25. Experimental results showing the transient response in load current, controller output, and step signal using by the PR controller ($K_p = 0.5$, and $K_i = 1000$).

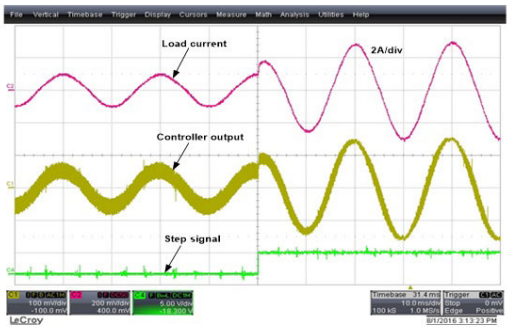

FIGURE 26. Experimental results showing the transient response in load current, controller output, and step signal using by the PR controller ($K_p = 0.7$, and $K_i = 2000$).

K_p beyond 0.6, the error value is increased. However, this value still significantly lower than the PI controller steady state error.

B. TRANSIENT RESPONSE OF PI AND PR CONTROLLER

The transient performance is examined by applying a step change in the current reference during normal conditions. Figure 22 (a) and (b) shows the simulation results for the step response in the load current using by the PI and PR controller, respectively. It can be seen that the PI controller is able to achieve a fast response to reach the steady-state condition, whereas the PR controller shows a fairly fast response that is comparable to the PI controller performance.

Figure 23 shows the experimental results of transient response in the load current, controller output, and step signal using by the PI controller for $K_p = 0.5$, $K_i = 200$. In all conditions, the current reference stepped from 1 A peak to 3.21 A peak. In each case, the results for the load current, controller output response, and step signal are shown in the figures.

From the analysis of transient response, the PI controller shows a reduced steady-state error when the value of K_p is increased from 0.5 to 0.7, and K_i is increased from 200 to 300 as shown in Figure 24, but this leads to over modulation causing increased ripple in the load current.

Figure 25 shows the experimental results of the transient response in the load current using by the PR controller for

$K_p = 0.5$, $K_i = 1000$. The transient response of PR controller is slightly slower where it takes a few cycles to reach the steady-state condition. But, it produces a higher output quality with very low current harmonics as compared to PI controller with high distortion especially at both positive and negative peak of the load current. This is also reflected by the smooth controller output response in PR as compared to that of PI controller shown in the figures.

For each case, the system is tested under different values of K_p, and K_i. It can be seen from the step response analysis that the controller response is faster when the K_p, and K_i are increased to 0.7 and 2000, respectively. Increasing the K_p and K_i to a higher value will cause more distortion as more harmonic components around the fundamental frequency are included as shown in Figure 26.

IX. CONCLUSION

In this paper, the performance of both PI and PR controls for a single-phase UPS inverter are presented through simulation and experimental results including the analysis of steady-state response, transient response, and output THD. Based on the test results, the obtained current THD of the PI controller is 6.37%, while low order current harmonics being attenuated and the measured 3rd and 5th order harmonics are 0.52 and 0.24, respectively. Note that the obtained current THD for the PR controller is 4.03%, again the low order current harmonics are also attenuated and the measured 3rd and 5th order harmonics are 0.35 and 0.22, respectively. These results demonstrate a significant improvement in current THD by the PR controller, with a 2.34% reduction.

REFERENCES

[1] M. I. Marei, I. Abdallah, and H. Ashour, "Transformerless uninterruptible power supply with reduced power device count," *Electr. Power Compon. Syst.*, vol. 39, no. 11, pp. 1097–1116, Jul. 2011.
[2] A. Nasiri, A. E. Amac, and A. Emadi, "Series-parallel active filter/uninterruptible power supply system," *Electr. Power Compon. Syst.*, vol. 32, no. 11, pp. 1151–1163, Nov. 2004.
[3] F. Blaabjerg and D. M. Ionel, "Renewable energy devices and systems—State-of-the-art technology, research and development, challenges and future trends," *Electr. Power Compon. Syst.*, vol. 43, no. 12, pp. 1319–1328, Jul. 2015.
[4] P. Mattavelli, "An improved deadbeat control for UPS using disturbance observers," *IEEE Trans. Ind. Electron.*, vol. 52, no. 1, pp. 206–212, Feb. 2005.
[5] F. Blaabjerg, R. Teodorescu, M. Liserre, and A. Timbus, "Overview of control and grid synchronization for distributed power generation systems," *IEEE Trans. Ind. Electron.*, vol. 53, no. 5, pp. 1398–1409, Oct. 2006.
[6] P. Cortes, G. Ortiz, J. I. Yuz, J. Rodriguez, S. Vazquez, and L. G. Franquelo, "Model predictive control of an inverter with output LC filter for UPS applications," *IEEE Trans. Ind. Electron.*, vol. 56, no. 6, pp. 1875–1883, Jun. 2009.
[7] H. Deng, R. Oruganti, and D. Srinivasan, "Analysis and design of iterative learning control strategies for UPS inverters," *IEEE Trans. Ind. Electron.*, vol. 54, no. 3, pp. 1739–1751, Jun. 2007.
[8] T.-L. Tai and J.-S. Chen, "UPS inverter design using discrete-time sliding-mode control scheme," *IEEE Trans. Ind. Electron.*, vol. 49, no. 1, pp. 67–75, Feb. 2002.
[9] J. Hu, L. Shang, Y. He, and Z. Q. Zhu, "Direct active and reactive power regulation of grid-connected DC/AC converters using sliding mode control approach," *IEEE Trans. Power Electron.*, vol. 26, no. 1, pp. 210–222, Jan. 2011.
[10] A. Benyoucef, K. Kara, A. Chouder, and S. Silvestre, "Prediction-based deadbeat control for grid-connected inverter with L-filter and LCL-filter," *Electr. Power Compon. Syst.*, vol. 42, no. 12, pp. 1266–1277, Sep. 2014.
[11] M. Parvez, M. Elias, N. Rahim, and N. Osman, "Current control techniques for three-phase grid interconnection of renewable power generation systems: A review," *Solar Energy*, vol. 135, pp. 29–42, Oct. 2016.
[12] P. Cortes, M. P. Kazmierkowski, R. M. Kennel, D. E. Quevedo, and J. Rodriguez, "Predictive control in power electronics and drives," *IEEE Trans. Ind. Electron.*, vol. 55, no. 12, pp. 4312–4324, Dec. 2008.
[13] M. Gálvez-Carrillo, R. De Keyser, and C. Ionescu, "Nonlinear predictive control with dead-time compensator: Application to a solar power plant," *Solar Energy*, vol. 83, no. 5, pp. 743–752, May 2009.
[14] W. Yan, J. Hu, V. Utkin, and L. Xu, "Sliding mode pulse width modulation," *IEEE Trans. Power Electron.*, vol. 23, no. 2, pp. 619–626, Mar. 2008.
[15] L. Schirone, F. Celani, and M. Macellari, "Discrete-time control for DC–AC converters based on sliding mode design," *IET Power Electron.*, vol. 5, no. 6, pp. 833–840, Jul. 2012.
[16] E. M. Navarro-López, D. Cortés, and C. Castro, "Design of practical sliding-mode controllers with constant switching frequency for power converters," *Electr. Power Syst. Res.*, vol. 79, no. 5, pp. 796–802, May 2009.
[17] H. Komurcugil, "Rotating-sliding-line-based sliding-mode control for single-phase UPS inverters," *IEEE Trans. Ind. Electron.*, vol. 59, no. 10, pp. 3719–3726, Oct. 2012.
[18] O. Kukrer, H. Komurcugil, and N. Bayindir, "Control strategy for single-phase UPS inverters," *IEE Proc., Electr. Power Appl.*, vol. 150, no. 6, p. 743, Dec. 2003.
[19] L. Malesani, L. Rossetto, G. Spiazzi, and A. Zuccato, "An AC power supply with sliding-mode control," *IEEE Ind. Appl. Mag.*, vol. 2, no. 5, pp. 32–38, Oct. 1996.
[20] R.-J. Wai and W.-H. Wang, "Grid-connected photovoltaic generation system," *IEEE Trans. Circuits Syst. I, Reg. Papers*, vol. 55, no. 3, pp. 953–964, Apr. 2008.
[21] S.-C. Tan, Y. Lai, and C. Tse, "Indirect sliding mode control of power converters via double integral sliding surface," *IEEE Trans. Power Electron.*, vol. 23, no. 2, pp. 600–611, Mar. 2008.
[22] M. Aamir, K. A. Kalwar, and S. Mekhilef, "Proportional-resonant and slide mode control for single-phase UPS inverter," *Electr. Power Compon. Syst.*, vol. 45, no. 1, pp. 11–21, Jan. 2017.
[23] A. Abrishamifar, A. Ahmad, and M. Mohamadian, "Fixed switching frequency sliding mode control for single-phase unipolar inverters," *IEEE Trans. Power Electron.*, vol. 27, no. 5, pp. 2507–2514, May 2012.
[24] M. Carpita and M. Marchesoni, "Experimental study of a power conditioning system using sliding mode control," *IEEE Trans. Power Electron.*, vol. 11, no. 5, pp. 731–742, Sep. 1996.
[25] S. Chiang, T. Tai, and T. Lee, "Variable structure control of UPS inverters," *IEE Proc., Electr. Power Appl.*, vol. 145, no. 6, p. 559, Nov. 1998.
[26] O. Kukrer, H. Komurcugil, and A. Doganalp, "A three-level hysteresis function approach to the sliding-mode control of single-phase UPS inverters," *IEEE Trans. Ind. Electron.*, vol. 56, no. 9, pp. 3477–3486, Sep. 2009.
[27] R. Teodorescu, F. Blaabjerg, M. Liserre, and P. Loh, "Proportional-resonant controllers and filters for grid-connected voltage-source converters," *IEE Proc., Electr. Power Appl.*, vol. 153, no. 5, p. 750, Mar. 2006.
[28] S. K. Gudey and R. Gupta, "Sliding-mode control in voltage source inverter-based higher-order circuits," *Int. J. Electron.*, vol. 102, no. 4, pp. 668–689, Apr. 2015.
[29] K. Zhang, Y. Kang, J. Xiong, and J. Chen, "Direct repetitive control of SPWM inverter for UPS purpose," *IEEE Trans. Power Electron.*, vol. 18, no. 3, pp. 784–792, May 2003.
[30] C. Rech, H. Pinheiro, H. Grundling, H. Hey, and J. Pinheiro, "A modified discrete control law for UPS applications," *IEEE Trans. Power Electron.*, vol. 18, no. 5, pp. 1138–1145, Sep. 2003.
[31] A. Timbus, M. Liserre, R. Teodorescu, P. Rodriguez, and F. Blaabjerg, "Evaluation of current controllers for distributed power generation systems," *IEEE Trans. Power Electron.*, vol. 24, no. 3, pp. 654–664, Mar. 2009.
[32] Y. Yang, K. Zhou, and F. Blaabjerg, "Current harmonics from single-phase grid-connected inverters—Examination and suppression," *IEEE J. Emerg. Sel. Topics Power Electron.*, vol. 4, no. 1, pp. 221–233, Mar. 2016.
[33] *IEEE Standard for Interconnecting Distributed Resources With Electric Power Systems*, IEEE Standard 1547-2003, Mar. 2009.

MOHAMMAD PARVEZ received the B.Sc. degree in electrical and electronic engineering from the Dhaka University of Engineering and Technology (DUET), Gazipur, Bangladesh, in 2010, and the M.Phil. degree in power electronics and control from the University of Malaya, Malaysia, in 2017. He is currently pursuing the Ph.D. degree from the School of Electrical and Electronic Engineering, The University of Adelaide, Australia. From 2011 to 2013, he worked at a 50 MW Peaking Power Plant as an Assistant Engineer (operation & maintenance), Comilla, Bangladesh. His research interests include grid-connected PV inverters, power electronics, renewable energy, and electrical drives.

MOHAMAD FATHI MOHAMAD ELIAS (Member, IEEE) received the B.Eng. (Hons.), M.Eng., and Ph.D. degrees in electrical engineering from the University of Malaya, Kuala Lumpur, Malaysia, in 2003, 2007, and 2013, respectively. He is currently a Senior Lecturer with the UM Power Energy Dedicated Advanced Centre, University of Malaya, Malaysia. His research interests include power electronics, renewable energy, and electrical drives.

NASRUDIN ABD RAHIM (Senior Member, IEEE) received the B.Sc. (Hons.) and M.Sc. degrees from the University of Strathclyde, Glasgow, U.K., and the Ph.D. degree from the Heriot–Watt University, Edinburgh, U.K., in 1995. He is currently a Professor with the University of Malaya, Kuala Lumpur, Malaysia, where he is also the Director of the UM Power Energy Dedicated Advanced Centre (UMPEDAC). He is also a Distinguish Adjunct Professor with the Renewable Energy Research Group, King Abdulaziz University, Jeddah, Saudi Arabia. His research interests include power electronics, solar PV and wind technologies, realtime control systems, and electrical drives. He is a Fellow of the Institution of Engineering and Technology, U.K., and the Academy of Sciences Malaysia. He is also a Chartered Engineer in U.K.

FREDE BLAABJERG (Fellow, IEEE) received the M.Sc. degree in EE from Aalborg University, Aalborg, Denmark, in 1987, and the Ph.D. degree from the Institute of Energy Technology, Aalborg University, in 1995. He was with ABB-Scandia, Randers, Denmark, from 1987 to 1988. He was an Assistant Professor with Aalborg University, in 1992, an Associate Professor, in 1996, and a Full Professor in power electronics and drives, in 1998. In 2006, he became the Dean of the Faculty of Engineering and Science, Aalborg University. He has authored or coauthored more than 500 publications in his research fields including the book *Control in Power Electronics* (Academic, 2002). His research areas are in power electronics, static power converters, ac drives, switched reluctance drives, modeling, characterization of power semiconductor devices and simulation, wind turbines, and green power inverters. During recent years, he has held a number of chair positions in research policy and research funding bodies in Denmark. He received the 1995 Angelos Award for his contribution in modulation technique and control of electric drives and the Annual Teacher Prize at Aalborg University, in 1995. In 1998, he received the Outstanding Young Power Electronics Engineer Award from the IEEE Power Electronics Society. He also received the C. Y. O'Connor Fellowship from Perth, Australia, in 2002, the Statoil Prize for his contributions to power electronics, in 2003, and the Grundfos Prize for his contributions to power electronics and drives, in 2004. He received 24 IEEE Prize Paper Awards, the IEEE PELS Distinguished Service Award, in 2009, the IEEE William E. Newell Power Electronics Award 2014, and the Villum Kann Rasmussen Research Award 2014. He is a 2019 Global Energy Prize Laureate and a 2020 IEEE Edison Medal Winner. He is an Associate Editor of the IEEE TRANSACTIONS ON INDUSTRY APPLICATIONS, the IEEE TRANSACTIONS ON POWER ELECTRONICS, the *Journal of Power Electronics*, and the Danish journal *Elteknik*. In 2006, he became the Editor-in-Chief of the IEEE TRANSACTIONS ON POWER ELECTRONICS. He was the Editor-in-Chief of the IEEE TRANSACTIONS ON POWER ELECTRONICS, from 2006 to 2012.

DEREK ABBOTT (Fellow, IEEE) was born in South Kensington, London, U.K., in 1960. He received the B.Sc. degree (Hons.) in physics from Loughborough University, Leicestershire, U.K., in 1982, and the Ph.D. degree in electrical and electronic engineering from The University of Adelaide, Adelaide, SA, Australia, in 1995, under the supervision of K. Eshraghian and B. R. Davis. From 1978 to 1986, he was a Research Engineer with the GEC Hirst Research Centre, London, U.K. From 1986 to 1987, he was a VLSI Design Engineer with Austek Microsystems, Australia. Since 1987, he has been with The University of Adelaide, where he is currently a Full Professor with the School of Electrical and Electronic Engineering. He co-edited the book *Quantum Aspects of Life* (London, U.K.: Imperial College Press, 2008), and coauthored *Stochastic Resonance* (Cambridge, U.K.: Cambridge University Press, 2012) and coauthored *Terahertz Imaging for Biomedical Applications,* (New York, NY, USA: Springer–Verlag, 2012). His interests are in the areas of multidisciplinary physics and electronic engineering applied to complex systems. His research programs span a number of areas of stochastics, game theory, photonics, renewable energy, energy policy, biomedical engineering, and computational neuroscience. He is a Fellow of the Institute of Physics (IoP), U.K. He has received a number of awards, including the Tall Poppy Award for Science, in 2004, an Australian Research Council Future Fellowship, in 2012, the David Dewhurst Medal, in 2015, the Barry Inglis Medal, in 2018, and the M. A. Sargent Medal, in 2019, for eminence in engineering. He has served as an Editor and/or Guest Editor for a number of journals, including the IEEE JOURNAL OF SOLID-STATE CIRCUITS, the *Journal of Optics B*, the *Microelectronics Journal*, *Chaos*, *Smart Structures and Materials*, *Fluctuation and Noise Letters*, the PROCEEDINGS OF THE IEEE, and the IEEE PHOTONICS JOURNAL. He is currently on the editorial boards of IEEE ACCESS, *Frontiers in Physics*, *Royal Society Open Science*, and Nature's *Scientific Reports*. He is currently also the Editor-in-Chief (EIC) of IEEE ACCESS and serves on the IEEE Publication Services and Products Board (PSPB).

SAID F. AL-SARAWI (Member, IEEE) received the general certificate in marine radio communication and the B.Eng. degree (Hons.) in marine electronics and communication from the Arab Academy for Science and Technology, Alexandria, Egypt, in 1987 and 1990, respectively, and the Ph.D. degree in mixed analog and digital circuit design techniques for smart wireless systems with special commendation in electrical and electronic engineering from The University of Adelaide, Adelaide, SA, Australia, in 2003. He also received the Graduate Certificate in education (higher education) The University of Adelaide, in 2006. He is currently the Director with the Centre for Biomedical Engineering and a Founding Member of the Education Research Group of Adelaide, The University of Adelaide. His research interests include design techniques for mixed signal systems in complementary metal–oxide–semiconductor and optoelectronic technologies for high-performance radio transceivers, low-power and low-voltage radio-frequency identification systems, data converters, mixed-signal design, and microelectromechanical systems for biomedical applications. His current educational research is focused on innovative teaching techniques for engineering education, research skill development, and factors affecting student's evaluations of courses in different disciplines. He received The University of Adelaide Alumni Postgraduate Medal (formerly Culross Prize) for outstanding academic merit at the postgraduate level. While pursuing the Ph.D. degree, he received the Commonwealth Postgraduate Research Award (Industry).